

pubs.acs.org/NanoLett Letter

Magnetic Effect of Dopants on Bright and Dark Excitons in Strongly Confined Mn-Doped CsPbl₃ Quantum Dots

Tian Qiao, Xiaohan Liu, Daniel Rossi, Mohit Khurana, Yulin Lin, Jianguo Wen, Jinwoo Cheon, Alexey V. Akimov, and Dong Hee Son*



Cite This: *Nano Lett.* 2021, 21, 9543–9550



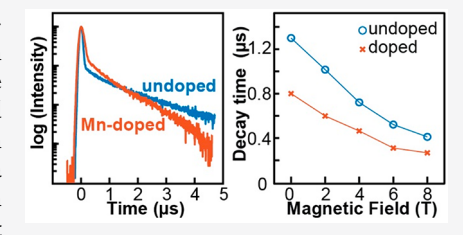
ACCESS

Metrics & More

Article Recommendations

s Supporting Information

ABSTRACT: We investigated the magnetic effect of Mn^{2+} ions on an exciton of Mndoped CsPbI₃ quantum dots (QDs), where we looked for the signatures of an exciton magnetic polaron known to produce a large effective magnetic field in Mn-doped CdSe QDs. In contrast to Mn-doped CdSe QDs that can produce ~100 T of magnetic field upon photoexcitation, manifested as a large change in the energy and relaxation dynamics of a bright exciton, Mn-doped CsPbI₃ QDs exhibited little influence of a magnetic dopant on the behavior of a bright exciton. However, a μ s-lived dark exciton in CsPbI₃ QDs showed 40% faster decay in the presence of Mn^{2+} , equivalent to the effect of ~3 T of an external magnetic field. While further study is necessary to fully



understand the origin of the large difference in the magneto-optic property of an exciton in two systems, we consider that the difference in antiferromagnetic coupling of the dopants is an important contributing factor.

KEYWORDS: Magnetic doping, quantum dot, exciton dynamics, dark exciton, perovskite

oping semiconductor nanocrystals (NCs) with paramagnetic ions introduces new pathways of energy exchange or coupling of different degrees of freedom, giving rise to new optical, electronic, and magneto-optic properties absent in undoped NCs. For example, dopant photoluminescence (PL), 1,2 circularly polarized exciton PL, 3,4 light or charge-induced magnetism, \$5-8\$ and generation of hot electrons via upconversion 9-13 were observed in II-VI or III-V NCs doped with Mn²⁺, Co²⁺, or Cu⁺. The efficiency of introducing new properties in doped NCs depends not only on the strength of the exciton-dopant interaction but also on other dynamic processes dissipating exciton population such as trapping of exciton by defects. 1,2,14 Therefore, significant effort has been made to understand the effect of varying the spatial distribution of exciton and dopant wave functions within the NCs and the competitive dynamics involving the relaxation of an exciton.

Recently, lead halide perovskite (LHP) NCs have emerged as a new material exhibiting the brighter exciton luminescence with higher defect tolerance than many other semiconductor NCs, ^{15–17} demonstrating their potential as the superior source of photons and charges. ^{18–23} Doping of various transition metal and rare earth elements was shown to be possible in both fully inorganic and organic—inorganic hybrid LHP NCs. ^{24–28} This opened the door to the use of LHP NCs as the host to obtain new photophysical properties resulting from the interaction of an exciton and a dopant, benefiting from their desirable photophysical properties. LHP NCs doped with Mn²⁺ ions are among the most extensively studied doped perovskite NCs. ^{29–36} While most studies in LHP NCs focused

on relatively large NCs with weak quantum confinement, recent progress in the synthesis of strongly quantum-confined LHP quantum dots (QDs) enabled investigating the confinement effect in perovskite QDs. For instance, strongly confined CsPbX₃ QDs have a facile access to intense and μ s-lived PL from the dark lowest-energy exciton at low temperatures in contrast to weakly or nonconfined NCs dominated by a bright exciton. Therefore, strong confinement of the host QDs not only provides a generally stronger exciton—dopant interaction but also enables utilizing both bright and dark exciton that may have different interactions with the dopant.

So far, studies in Mn-doped CsPbX $_3$ QDs have focused primarily on the role of Mn $^{2+}$ ions as the source of sensitized photons, while Mn $^{2+}$ ions can potentially create a magnetic field that alters the behavior of the exciton through Zeeman effect and magnetic mixing of bright and dark excitons. ^{40,41} In Mn-doped CdSe QDs, a large effective magnetic field (\sim 100 T for 4.7 nm CdSe QD with 1.4% Mn doping) was observed from the formation of an exciton magnetic polaron (EMP). However, whether a large effective magnetic field can be produced via EMP in Mn-doped CsPbX $_3$ QDs as in Mn-doped CdSe QDs still remains largely uninvestigated. To this end, we

Received: August 12, 2021 Revised: November 5, 2021 Published: November 11, 2021





studied the effect of a Mn²⁺ dopant on the energetics and dynamics of bright and dark exciton PL in strongly confined Mn-doped CsPbI₃ QDs and looked for the spectroscopic signatures of EMP. We chose strongly confined Mn-doped CsPbI₃ QDs with sufficiently low bandgap without exciton—Mn energy transfer, since the potential EMP formation and exciton relaxation dynamics are not disrupted by the sensitization of Mn, while simultaneously providing the quantum confinement.⁴²

The analysis of the time-dependent exciton PL spectra at various temperatures and external magnetic fields showed that Mn doping accelerates the decay of a dark exciton while the effect on a bright exciton is insignificant. The temperaturedependent Stokes shift and spectral dynamics of a bright exciton suggested that EMP similar to that of Mn-doped CdSe QDs creating a large effective magnetic field is not formed in Mn-doped CsPbI₃ QDs. 4,6 Despite the similarity between Mndoped CsPbX₃ QDs and Mn-doped II-VI QDs in their ability to sensitize Mn PL, the exciton-dopant interaction relevant for creating EMP appears quite different in CsPbI3 and CdSe QDs. While further studies are necessary to fully understand the origin of this difference, the results from this study suggest that the difference in the degree of antiferromagnetic coupling of dopants in CsPbI₃ and CdSe QDs may be an important contributing factor.

Figure 1 shows transmission electron microscopy (TEM) images (a-d), absorption and PL spectra (e), and time-

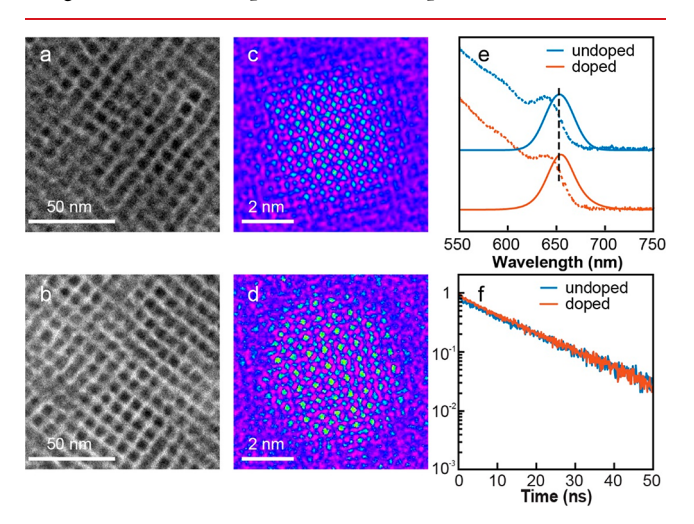


Figure 1. TEM images of undoped CsPbI₃ QDs (a, c) and 3.0% Mndoped CsPbI₃ QDs (b, d). (e) Room-temperature absorption (dashed line) and PL (solid line) spectra of undoped and Mn-doped and CsPbI₃ QDs dispersed in hexane. (f) Time-dependent exciton PL intensities of undoped and Mn-doped CsPbI₃ QDs dispersed in hexane at room temperature.

dependent exciton PL intensities (f) of 3.0% Mn-doped and undoped CsPbI₃ QDs at room temperature. Both Mn-doped and undoped QDs have a similar edge length of 6.5 nm, which is much smaller than the exciton Bohr diameter of CsPbI₃ (12 nm). Aberration-corrected high resolution TEM images (Figure 1c,d) indicate that doping Mn²⁺ ions in CsPbI₃ QDs studied here does not introduce a noticeable change in the lattice structure, consistent with very similar X-ray diffraction patterns of Mn-doped and undoped CsPbI₃ QDs. (Figure S1) Details of the synthesis, structural, and chemical character-

ization and spectroscopic measurements are in Supporting Information.

Both Mn-doped and undoped CsPbI₃ QDs exhibit similar quantum-confined exciton absorption and emission spectra blue-shifted by \sim 0.2 eV with respect to bulk.^{15,43} Both QDs exhibit comparable exciton PL quantum yield (\sim 85%) and PL lifetime (14 ns) in solution at room temperature, indicating little influence of the dopant on the pathways of exciton relaxation and charge carrier trapping. Earlier studies reported that heavy Mn doping in CsPbX₃ (X = Cl, Br) NCs increase the bandgap unrelated to quantum confinement due to the alloying within the host NCs.^{34,36} On the one hand, the effect of Mn doping in CsPbI₃ QDs at the level of this study (<3.0%) on the bandgap is insignificant. On the other hand, Mn doping increases the long-term stability of the host QDs, suppressing the transformation to yellow phase occurring in undoped CsPbI₃ QD (Figure S2), similarly to what was observed in the alloyed CsPb_xMn_{1-x}I₃ NCs with high Mn content (9%).⁴³

Because of the absence of the sensitized Mn PL, visual confirmation of doping is difficult for Mn-doped CsPbI₃ QDs. More direct confirmation of Mn doping is obtained from the magnetization curves measured with superconducting quantum interference device (SQUID) as shown in Figure 2a. In

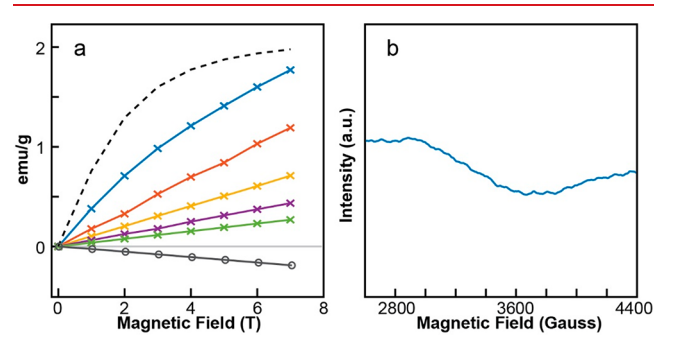


Figure 2. (a) Magnetization curve of 3.0% Mn-doped (solid curve with X) and undoped (solid curve with O) CsPbI₃ QDs. For Mn-doped QDs, the temperature is 4, 20, 50, 100, and 200 K respectively from top to bottom. The dashed curve is from Brillouin function for S = 5/2 at 4 K, with saturation magnetization set at 2.1 emu/g for the comparison of saturation behavior only. (b) EPR spectrum of 3.0% Mn-doped CsPbI₃ QDs at room temperature.

contrast to undoped CsPbI₃ QDs that exhibit weak and temperature-independent diamagnetic behavior, Mn-doped CsPbI₃ QDs exhibit paramagnetic behavior due to the dopant. However, the magnetization curve at 4 K saturates much more slowly with increasing magnetic field than what the Brillouin function (eq 1) predicts for noninteracting Mn^{2+} ions with spin S = 5/2.

$$M \propto \left[(2S+1) \coth \left((2S+1) \left(\frac{g\mu_{\rm B}H}{2kT} \right) \right) - \coth \left(\frac{g\mu_{\rm B}H}{2kT} \right) \right]$$
(1)

Fitting the magnetization curve at 4 K to eq 1 with a g value of 2.0 gives S < 1, much smaller than 5/2, indicating a significant antiferromagnetic interaction among Mn^{2+} ions within the QDs. The room-temperature electron paramagnetic resonance (EPR) spectrum of Mn-doped CsPbI₃ QDs shown in Figure 2b lacks a well-resolved fine structure previously seen in Mn-doped CsPbCl₃ QDs, 29,44 consistent with substantial

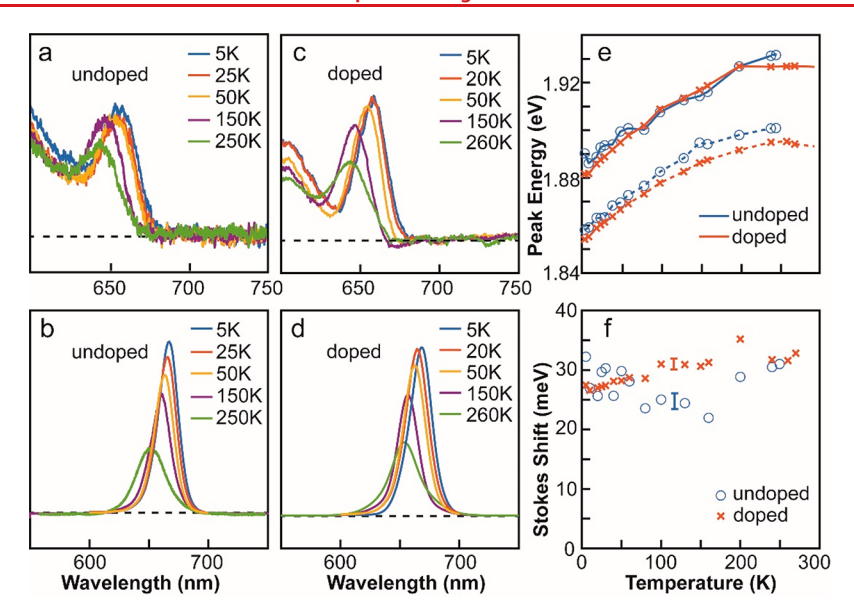


Figure 3. (a, b) Absorption and PL spectra of undoped CsPbI₃ QDs at various temperatures. (c, d) Absorption and PL spectra of 3.0% Mn-doped CsPbI₃ QDs at various temperatures. (e) Temperature-dependent absorption (solid) and PL (dashed) peak energy of Mn-doped and undoped CsPbI₃ QDs. (f) Temperature-dependent Stokes shift of Mn-doped and undoped CsPbI₃ QDs. Error bars represent the average uncertainties in Stokes shift measurement.

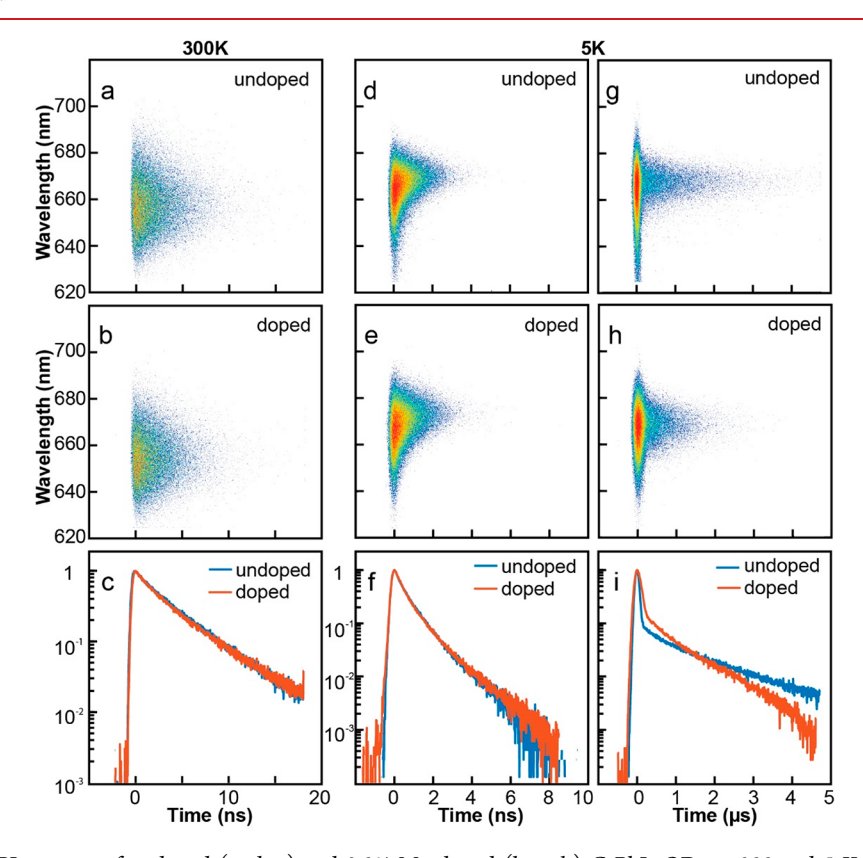


Figure 4. Time-resolved PL spectra of undoped (a, d, g) and 3.0% Mn-doped (b, e, h) CsPbI₃ QDs at 300 and 5 K. At 5 K, time-resolved PL spectra are presented in 10 ns and 5 μ s time windows to show both bright and dark exciton PL more clearly. (c, f, i) Time-dependent PL intensities of Mn-doped and undoped CsPbI₃ QDs at 300 K (c) and 5 K (f, i).

antiferromagnetic coupling of Mn²⁺ ions. Further details on EPR measurements are in Supporting Information.

To examine the effect of Mn doping on the energetics and dynamics of exciton in CsPbI₃ QDs, temperature-dependent steady-state absorption and PL spectra and time-dependent PL spectra were obtained. Figure 3a–d show the absorption and

PL spectra of Mn-doped and undoped CsPbCl₃ QDs dispersed in polystyrene film at various temperatures. Panels e and f of Figure 3 show the temperature-dependent absorption and PL peak energies and Stokes shift, respectively. Both Mn-doped and undoped CsPbI₃ QDs show a similar redshift of the exciton absorption and PL peaks with decreasing temperature,

with relatively weak temperature dependence of the Stokes shift.

Earlier studies in Mn-doped CdSe QDs showed the formation of EMP with a large effective magnetic field ($\sim 10^2$ T at 5 K), which redshifts the steady-state PL at 5 K by several hundreds of meV compared with undoped QDs from the Zeeman splitting of exciton levels. The EMP formation time was estimated to be 50-500 ps from the dynamic redshift of the PL in Mn-doped CdSe QDs during the first several ns that is absent in undoped CdSe QDs. In CsPbX₃ QDs, bright and dark excitons are reported to have a total angular momentum of I = 1 and 0 respectively. ^{41,45,46} Although bright exciton of CsPbI₃ QDs decays in ~1 ns at 5 K, PL peak shift of the bright exciton should still be observable if EMP forms from bright exciton faster than ~1 ns. However, no significant difference is observed in the steady-state PL peak energy and Stokes shift at 5 K between Mn-doped and undoped CsPbI₃ QDs. Furthermore, the dynamic Stokes shift of the bright exciton at 5 K is also nearly identical for Mn-doped and undoped QDs as will be discussed shortly. These indicate that EMP similar to that of Mn-doped CdSe QDs is not formed in Mn-doped CsPbI₃ QDs, suggesting a significant difference in the exciton dopant interaction responsible for the formation of EMP between these two QDs.

In order to further examine the effect of Mn²⁺ ions on the energetics and dynamics of both bright and dark excitons, time-resolved PL spectra of Mn-doped and undoped QDs were obtained at various temperatures under weak pulsed 405 nm excitation (details in Supporting Information). Figure 4 compares the time-resolved PL spectra and time-dependent PL intensities of Mn-doped and undoped CsPbI₃ QDs at 300 and 5 K. At 300 K, the PL is entirely from a bright exciton that decays single exponentially in both Mn-doped and undoped QDs. Mn²⁺ ions have a negligible effect on the relaxation rate of a bright exciton, although the PL lifetime is shorter (4.4 ns in vacuum and 2.5 ns in air) than in solution samples. The shorter PL lifetime of the QDs in polymer film compared with in solution was attributed to the loss of the surface ligands promoting the nonradiative decay. 47,48 The absence of the effect of doped Mn2+ ions on PL lifetime continues down to ~100 K, while the difference in PL decay in Mn-doped and undoped QDs begins to become more apparent below 50 K (Figure S3).

At 5 K, the PL decays on two very different time scales. The average time constants for the fast (τ_F) and slow (τ_S) component of the decay are on subns and μ s scale respectively as summarized in Table 1. While both τ_F and τ_S vary with

Table 1. PL Decay Times of Undoped and 3.0% Mn-Doped CsPbI₃ QDs at 300 and 5 K under Vacuum

	300 K	5 K	
sample	τ (ns)	$\tau_{\mathrm{F}} \; (\mathrm{ns})$	$\tau_{\rm S}~(\mu{\rm s})$
undoped	4.4	0.82	1.3
doped (3.0%)	4.4	0.82	0.8

temperature, they are interpreted as the decay of a bright and a dark exciton, respectively, at sufficiently low temperatures suppressing the thermal excitation from dark to bright state as has been shown in our recent studies in $CsPbX_3$ (X = Br, I) QDs. 38,39 To show the decay dynamics of both bright and dark exciton PL at 5 K more clearly, the time-resolved PL data are presented in two different time windows in Figure 4d—i.

The fast-decay component of the PL at 5 K shown in Figure 4d—f has contributions from both the relaxation of the initially photoexcited bright exciton and bright-to-dark transition. The decay time constant ($\tau_{\rm F}=0.82~{\rm ns}$) is nearly identical for both Mn-doped and undoped QDs. The time-dependent redshift of bright exciton PL (Figure S4) is also similar. While the exact origin of this shift is not entirely clear, we tentatively attribute it to slow cooling from the initially excited state with 405 nm photon. The similarity of the spectral and PL decay dynamics of the bright exciton in conjunction with the similar temperature-dependent Stokes shift (Figure 3f) in Mn-doped and undoped CsPbI₃ QDs is consistent with the absence of the strong internal magnetic field from EMP.

On the other hand, the slow-decay component (τ_S) of the PL at 5 K shown in Figure 4g-i, reflecting the relaxation of dark exciton, shows a distinct difference between Mn-doped and undoped QDs. 40% shorter τ_S in Mn-doped QDs can in principle be interpreted as the faster radiative decay (e.g., from increased oscillator strength) or the faster nonradiative decay (e.g., due to trapping of dark exciton). However, more efficient nonradiative decay in Mn-doped QDs than in undoped QDs is unlikely for the following reasons. First, the decay time of the initially photoexcited bright exciton (τ_E) , from which the dark exciton level is populated, is not sensitive to doping both at 5 and 300 K as shown in Figure 4c,f, indicating that doping does not introduce an additional thermally activated nonradiative pathway for bright exciton. Second, the possible presence of a deep trap with high thermal detrapping barrier that may affect only the slowly decaying dark exciton is ruled out, because the PL decay time of bright exciton is nearly identical for both Mndoped and undoped QDs in a very broad range of temperatures (50-300 K) (Figure S3). Therefore, we consider more efficient nonradiative decay by doping is unlikely to be the reason for the faster decay of dark exciton PL in Mn-doped QDs. We also ruled out the increase of the oscillator strength by the localization of exciton wave function. An earlier study in Mn-doped CsPb(Cl/Br)₃ QDs reported the possible localization of exciton by the dopant, leading to the increase in the oscillator strength of exciton and faster sensitization of Mn PL at room temperature. 49 However, absorption cross sections of Mn-doped and undoped CsPbI₃ QDs at room temperature determined employing the elemental analysis method are nearly identical. 50,51 (Figure S5) This indicates the absence of the dopant-induced exciton localization in Mn-doped CsPbI₃ QDs altering the oscillator strength of exciton.

Another explanation for the faster relaxation of a dark exciton is mixing of bright and dark exciton states by the external perturbation such as magnetic field. Studies in several LHP NCs reported the shortening of dark exciton lifetime from magnetic mixing of bright and dark excitons that increases the oscillator strength of the dark exciton. 38,41,52,53 Since accelerating the dark exciton PL decay from 1.3 to 0.8 μ s by borrowing the oscillator strength from bright exciton should not take much oscillator strength from the bright exciton, little difference in the bright exciton PL decay time between Mndoped and undoped QDs is consistent with this scenario. The steady-state PL and dynamics of bright exciton PL discussed above indicate the absence of EMP similar to that of Mndoped CdSe QDs. However, the photoexcited Mn-doped CsPbI₃ QDs may still generate the weaker effective magnetic field that can alter the dark exciton lifetime via magnetic mixing.

To gain additional insights into the effect of Mn²⁺ on the relaxation of dark exciton, the decay of dark exciton PL from Mn-doped and undoped CsPbI₃ QDs were compared under varying external magnetic field at 5 K. Figure 5a,b show the

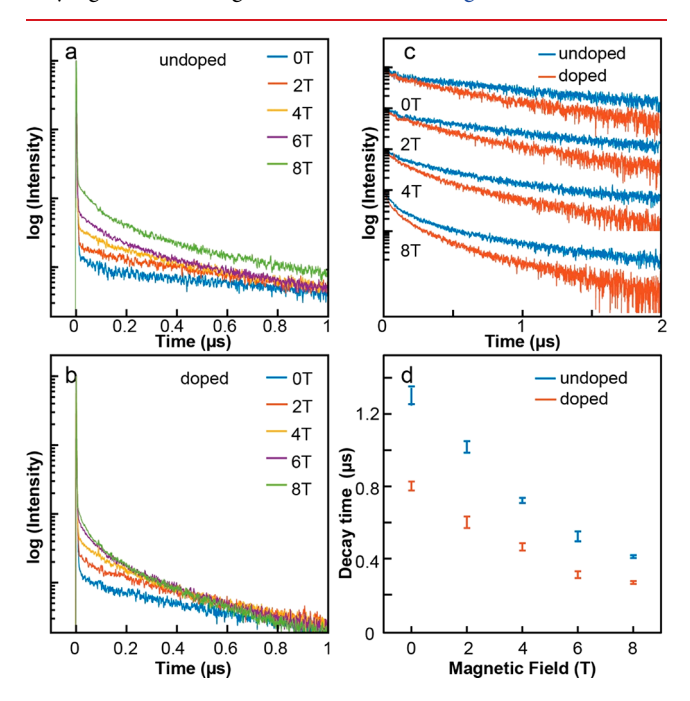


Figure 5. (a, b) Time-dependent exciton PL intensity of undoped (a) and 3.0% Mn-doped (b) CsPbI₃ QDs under the external magnetic field at 5 K. (c) Comparison of the isolated dark exciton PL decay components in undoped and 3.0% Mn-doped QDs under the external magnetic field. (d) Dark exciton PL decay times in undoped and 3.0% Mn-doped QDs under the external magnetic field.

normalized time-dependent PL intensity as a function of external magnetic field in 0-8 T range in Faraday geometry for undoped and 3.0% Mn-doped CsPbI₃ QDs, respectively (details in Supporting Information). With increasing external magnetic field, dark exciton PL decays faster for both Mndoped and undoped CsPbI₃ QDs. For clarity, the dark exciton component of the PL decay is isolated and compared in Figure 5c after normalization to the peak amplitude at several different magnetic fields. Figure 5d shows the average decay time of dark exciton PL from Mn-doped and undoped QDs under 0-8 T of magnetic field at 5 K. The data in Figure 5d indicate that the effect of doping Mn²⁺ on dark exciton PL decay is equivalent to an additional 3-3.5 T of magnetic field in undoped QDs if the shortening of the dark exciton lifetime is of magnetic origin. This requires that the effective magnetic field should sustain on the time scale of dark exciton lifetime or longer, which can be possible if the weak effective magnetic field is from "weak" EMP formed from dark exciton. However, a dark exciton with J = 0 renders the Stokes shift less informative as a signature for the magnetic field created by the dark exciton interacting with dopants. More direct confirmation of whether a dark exciton can create an effective magnetic field will require time-resolved measurement of the magnetization with pulsed optical excitation. Interestingly, a recent study in Mn-doped 2D Ruddlesden-Popper hybrid perovskite also reported the acceleration of dark exciton PL decay by Mn²⁺ ions, although it is speculative about its exact mechanism.

The large difference in the ability to generate effective magnetic field via EMP between Mn-doped CsPbI₃ and CdSe QDs is intriguing, considering that the ability to sensitize Mn PL in Mn-doped CsPbX₃ (X = Cl, Cl/Br) NCs is not markedly different from Mn-doped II-VI QDs. A comparison in Mndoped CsPbCl3 and Mn-doped CdS/ZnS QDs indicated that the exciton-Mn energy transfer is a few times slower in CsPbCl₃ than in CdS/ZnS host QDs of the comparable size and doping concentration. 55 If the sensitization of Mn PL and the formation of EMP are mediated by the same type of exciton-dopant exchange interaction, one would expect the difference in the ability to form EMP in two different host QDs be comparable to that of sensitization of the dopant PL. Such simple extrapolation fails to explain the large difference in the spectroscopic signatures reflecting the effective magnetic field from dopant in Mn-doped CsPbI₃ QDs and Mn-doped CdSe QDs. This suggests that there is a significant difference in the magnitude of charge carrier-dopant exchange interaction or/ and interaction among dopants within the QDs between Mndoped CsPbI3 and Mn-doped CdSe QDs. One potential contribution may be the difference in the degree of antiferromagnetic coupling of Mn2+ ions within CsPbI3 and II–VI host QDs. Recent studies showed that Mn²⁺ clustering can occur in CsPbCl_xBr_{3-x} nanocrystals at higher doping concentration or during the anion exchange, reducing the EPR signal due to antiferromagnetic coupling, 44,56 which may also be possible in CsPbI₃ QDs studied here. This contrasts to Mndoped CdSe QDs with comparable doping concentration exhibiting much more well-defined EPR signal with clearly resolvable hyperfine structure, 57 suggesting less extensive antiferromagnetic coupling in CdSe than in CsPbI₃ host. To examine the effect of decreasing doping concentration on the spin interaction of Mn²⁺ that may potentially alter the ability to form EMP, additional measurements of the magnetization curves and time-dependent PL under the external magnetic field were made on 0.5% Mn-doped CsPbI₃ QDs. Figure S6 compares the optical spectra, EPR data, magnetization curves and magnetic field-dependent dark exciton PL decay of 0.5% and 3.0% Mn-doped CsPbI₃ QDs. Magnetization curves indicate that Mn²⁺ ions exhibit comparable antiferromagnetic coupling at both Mn doping concentrations, with very similar shape of the mass magnetization vs magnetic field curves. Dark exciton PL decay of 0.5% Mn-doped CsPbI₃ QDs at 5 K is also in between those of undoped and 3.0% Mn-doped CsPbI₃ QDs. These indicate that the antiferromagnetic coupling of Mn²⁺ ions in CsPbI₃ QDs is substantial even at relatively low (0.5%) doping concentration, unlike in the CdSe host. Certainly, knowledge on the strength of exciton—Mn exchange interaction in CsPbI3 relative to other hosts and detailed doping structure will be necessary to gain a complete understanding of the origin of the large difference between Mn-doped CsPbX₃ and II-VI QDs.

In conclusion, we investigated the effect of doping paramagnetic Mn^{2+} ions in strongly quantum confined CsPbI_3 QDs on the energetics and dynamics of bright and dark exciton. While doping Mn^{2+} ions has little influence on the spectral and PL decay dynamics of a bright exciton, it accelerates the decay of a dark exciton significantly. We attribute this difference to the magnetic mixing of bright and dark excitons, whose effect is equivalent to $\sim\!3$ T of external magnetic field. However, the spectroscopic data indicates that formation of EMP similar to that observed in Mn-doped CdSe QDs, producing very large ($\sim\!10^2$ T) effective magnetic field, is

not formed in CsPbI₃ QDs. While further studies are necessary, we conjecture that more extensive antiferromagnetic coupling of Mn²⁺ ions in CsPbI₃ QDs is partially responsible for much weaker ability to produce EMP compared with Mndoped CdSe QDs.

ASSOCIATED CONTENT

Supporting Information

The Supporting Information is available free of charge at https://pubs.acs.org/doi/10.1021/acs.nanolett.1c03114.

Details of the synthesis, time-resolved and static PL at varying temperature and magnetic field, SQUID, EPR, TEM and absorption cross section measurements, additional temperature-dependent PL spectra, comparison of 0.5% and 3.0% Mn-doped CsPbI₃ QD data (PDF)

AUTHOR INFORMATION

Corresponding Author

Dong Hee Son — Department of Chemistry, Texas A&M University, College Station, Texas 777843, United States; Center for Nanomedicine, Institute for Basic Science and Graduate Program of Nano Biomedical Engineering, Advanced Science Institute, Yonsei University, Seoul 03722, Republic of Korea; orcid.org/0000-0001-9002-5188; Email: dhson@chem.tamu.edu

Authors

Tian Qiao — Department of Chemistry, Texas A&M University, College Station, Texas 777843, United States; orcid.org/0000-0002-0299-354X

Xiaohan Liu — Department of Physics, Texas A&M University, College Station, Texas 777843, United States

Daniel Rossi — Center for Nanomedicine, Institute for Basic Science and Graduate Program of Nano Biomedical Engineering, Advanced Science Institute, Yonsei University, Seoul 03722, Republic of Korea

Mohit Khurana – Department of Physics, Texas A&M University, College Station, Texas 777843, United States

Yulin Lin – Center for Nanoscale Materials, Argonne National Laboratory, Argonne, Illinois 60439, United States

Jianguo Wen — Center for Nanoscale Materials, Argonne National Laboratory, Argonne, Illinois 60439, United States; o orcid.org/0000-0002-3755-0044

Jinwoo Cheon — Center for Nanomedicine, Institute for Basic Science and Graduate Program of Nano Biomedical Engineering, Advanced Science Institute, Yonsei University, Seoul 03722, Republic of Korea; ⊚ orcid.org/0000-0001-8948-5929

Alexey V. Akimov — Department of Physics, Texas A&M University, College Station, Texas 777843, United States; orcid.org/0000-0002-4167-5085

Complete contact information is available at: https://pubs.acs.org/10.1021/acs.nanolett.1c03114

Author Contributions

[¶]T.Q. and X.L. contributed equally to this work.

Notes

The authors declare no competing financial interest.

ACKNOWLEDGMENTS

D.H.S. and A.A. acknowledge the National Science Foundation (CHE-2003961), Welch Foundation (A-1639) and X-grants from Texas A&M University for financial support. J.C. acknowledges Institute for Basic Science (IBS-R026-D1) for financial support. The authors thank Dr. Nattamai Bhuvanesh for assistance with XRD, Dr. Trevor Latendresse with SQUID, Trevor Latendresse, Dr. Vladimir Bakhmoutov and Dr. David Powers for EPR measurement. Use of the Center for Nanoscale Materials, an Office of Science user facility, was supported by the U.S. Department of Energy, Office of Science, Office of Basic Energy Sciences, under Contract No. DE-AC02-06CH11357.

REFERENCES

- (1) Yang, Y.; Chen, O.; Angerhofer, A.; Cao, Y. C. Radial-Position-Controlled Doping of CdS/ZnS Core/Shell Nanocrystals: Surface Effects and Position-Dependent Properties. *Chem. Eur. J.* **2009**, *15* (13), 3186–3197.
- (2) Chen, H.-Y.; Maiti, S.; Son, D. H. Doping Location-Dependent Energy Transfer Dynamics in Mn-Doped CdS/ZnS Nanocrystals. *ACS Nano* **2012**, *6* (1), 583–591.
- (3) Beaulac, R.; Archer, P. I.; Liu, X.; Lee, S.; Salley, G. M.; Dobrowolska, M.; Furdyna, J. K.; Gamelin, D. R. Spin-Polarizable Excitonic Luminescence in Colloidal Mn²⁺-Doped CdSe Quantum Dots. *Nano Lett.* **2008**, *8* (4), 1197–1201.
- (4) Nelson, H. D.; Bradshaw, L. R.; Barrows, C. J.; Vlaskin, V. A.; Gamelin, D. R. Picosecond Dynamics of Excitonic Magnetic Polarons in Colloidal Diffusion-Doped Cd_{1-x}Mn_xSe Quantum Dots. *ACS Nano* **2015**, *9* (11), 11177–11191.
- (5) Archer, P. I.; Santangelo, S. A.; Gamelin, D. R. Direct Observation of sp—d Exchange Interactions in Colloidal Mn²⁺- and Co²⁺-Doped CdSe Quantum Dots. *Nano Lett.* **2007**, *7* (4), 1037—1043.
- (6) Beaulac, R.; Schneider, L.; Archer, P. I.; Bacher, G.; Gamelin, D. R. Light-Induced Spontaneous Magnetization in Doped Colloidal Quantum Dots. *Science* **2009**, *325* (5943), 973–976.
- (7) Pandey, A.; Brovelli, S.; Viswanatha, R.; Li, L.; Pietryga, J. M.; Klimov, V. I.; Crooker, S. A. Long-lived photoinduced magnetization in copper-doped ZnSe-CdSe core-shell nanocrystals. *Nat. Nanotechnol.* **2012**, *7* (12), 792–797.
- (8) Ochsenbein, S. T.; Feng, Y.; Whitaker, K. M.; Badaeva, E.; Liu, W. K.; Li, X.; Gamelin, D. R. Charge-controlled magnetism in colloidal doped semiconductor nanocrystals. *Nat. Nanotechnol.* **2009**, 4 (10), 681–687.
- (9) Chen, H.-Y.; Chen, T.-Y.; Berdugo, E.; Park, Y.; Lovering, K.; Son, D. H. Hot Electrons from Consecutive Exciton—Mn Energy Transfer in Mn-Doped Semiconductor Nanocrystals. *J. Phys. Chem. C* **2011**, *115* (23), 11407—11412.
- (10) Dong, Y.; Parobek, D.; Rossi, D.; Son, D. H. Photoemission of Energetic Hot Electrons Produced via Up-Conversion in Doped Quantum Dots. *Nano Lett.* **2016**, *16* (11), 7270–7275.
- (11) Dong, Y.; Rossi, D.; Parobek, D.; Son, D. H. Nonplasmonic Hot-Electron Photocurrents from Mn-Doped Quantum Dots in Photoelectrochemical Cells. *ChemPhysChem* **2016**, *17* (5), 660–664. (12) Barrows, C. J.; Rinehart, J. D.; Nagaoka, H.; deQuilettes, D. W.; Salvador, M.; Chen, J. I. L.; Ginger, D. S.; Gamelin, D. R. Electrical Detection of Quantum Dot Hot Electrons Generated via a Mn²⁺-Enhanced Auger Process. *J. Phys. Chem. Lett.* **2017**, *8* (1), 126–130.
- (13) Singh, R.; Liu, W.; Lim, J.; Robel, I.; Klimov, V. I. Hot-electron dynamics in quantum dots manipulated by spin-exchange Auger interactions. *Nat. Nanotechnol.* **2019**, *14* (11), 1035–1041.
- (14) Maiti, S.; Chen, H.-Y.; Park, Y.; Son, D. H. Evidence for the Ligand-Assisted Energy Transfer from Trapped Exciton to Dopant in Mn-Doped CdS/ZnS Semiconductor Nanocrystals. *J. Phys. Chem. C* **2014**, *118* (31), 18226–18232.

- (15) Protesescu, L.; Yakunin, S.; Bodnarchuk, M. I.; Krieg, F.; Caputo, R.; Hendon, C. H.; Yang, R. X.; Walsh, A.; Kovalenko, M. V. Nanocrystals of Cesium Lead Halide Perovskites (CsPbX₃, X = Cl, Br, and I): Novel Optoelectronic Materials Showing Bright Emission with Wide Color Gamut. *Nano Lett.* **2015**, *15* (6), 3692–3696.
- (16) Koscher, B. A.; Swabeck, J. K.; Bronstein, N. D.; Alivisatos, A. P. Essentially Trap-Free CsPbBr₃ Colloidal Nanocrystals by Postsynthetic Thiocyanate Surface Treatment. *J. Am. Chem. Soc.* **2017**, *139* (19), 6566–6569.
- (17) Kang, J.; Wang, L.-W. High Defect Tolerance in Lead Halide Perovskite CsPbBr₃. J. Phys. Chem. Lett. **2017**, 8 (2), 489–493.
- (18) Utzat, H.; Sun, W.; Kaplan, A. E. K.; Krieg, F.; Ginterseder, M.; Spokoyny, B.; Klein, N. D.; Shulenberger, K. E.; Perkinson, C. F.; Kovalenko, M. V.; Bawendi, M. G. Coherent single-photon emission from colloidal lead halide perovskite quantum dots. *Science* **2019**, 363 (6431), 1068–1072.
- (19) Dong, Y.; Wang, Y.-K.; Yuan, F.; Johnston, A.; Liu, Y.; Ma, D.; Choi, M.-J.; Chen, B.; Chekini, M.; Baek, S.-W.; Sagar, L. K.; Fan, J.; Hou, Y.; Wu, M.; Lee, S.; Sun, B.; Hoogland, S.; Quintero-Bermudez, R.; Ebe, H.; Todorovic, P.; Dinic, F.; Li, P.; Kung, H. T.; Saidaminov, M. I.; Kumacheva, E.; Spiecker, E.; Liao, L.-S.; Voznyy, O.; Lu, Z.-H.; Sargent, E. H. Bipolar-shell resurfacing for blue LEDs based on strongly confined perovskite quantum dots. *Nat. Nanotechnol.* 2020, 15 (8), 668–674.
- (20) Li, G.; Rivarola, F. W. R.; Davis, N. J. L. K.; Bai, S.; Jellicoe, T. C.; de la Peña, F.; Hou, S.; Ducati, C.; Gao, F.; Friend, R. H.; Greenham, N. C.; Tan, Z.-K. Highly Efficient Perovskite Nanocrystal Light-Emitting Diodes Enabled by a Universal Crosslinking Method. *Adv. Mater.* **2016**, 28 (18), 3528–3534.
- (21) Swarnkar, A.; Marshall, A. R.; Sanehira, E. M.; Chernomordik, B. D.; Moore, D. T.; Christians, J. A.; Chakrabarti, T.; Luther, J. M. Quantum dot—induced phase stabilization of α -CsPbI₃ perovskite for high-efficiency photovoltaics. *Science* **2016**, *354* (6308), 92–95.
- (22) Jena, A. K.; Kulkarni, A.; Miyasaka, T. Halide Perovskite Photovoltaics: Background, Status, and Future Prospects. *Chem. Rev.* **2019**, *119* (5), 3036–3103.
- (23) Dey, A.; Ye, J.; De, A.; Debroye, E.; Ha, S. K.; Bladt, E.; Kshirsagar, A. S.; Wang, Z.; Yin, J.; Wang, Y.; Quan, L. N.; Yan, F.; Gao, M.; Li, X.; Shamsi, J.; Debnath, T.; Cao, M.; Scheel, M. A.; Kumar, S.; Steele, J. A.; Gerhard, M.; Chouhan, L.; Xu, K.; Wu, X.-g.; Li, Y.; Zhang, Y.; Dutta, A.; Han, C.; Vincon, I.; Rogach, A. L.; Nag, A.; Samanta, A.; Korgel, B. A.; Shih, C.-J.; Gamelin, D. R.; Son, D. H.; Zeng, H.; Zhong, H.; Sun, H.; Demir, H. V.; Scheblykin, I. G.; Mora-Seró, I.; Stolarczyk, J. K.; Zhang, J. Z.; Feldmann, J.; Hofkens, J.; Luther, J. M.; Pérez-Prieto, J.; Li, L.; Manna, L.; Bodnarchuk, M. I.; Kovalenko, M. V.; Roeffaers, M. B. J.; Pradhan, N.; Mohammed, O. F.; Bakr, O. M.; Yang, P.; Müller-Buschbaum, P.; Kamat, P. V.; Bao, Q.; Zhang, Q.; Krahne, R.; Galian, R. E.; Stranks, S. D.; Bals, S.; Biju, V.; Tisdale, W. A.; Yan, Y.; Hoye, R. L. Z.; Polavarapu, L. State of the Art and Prospects for Halide Perovskite Nanocrystals. ACS Nano 2021, 15 (7), 10775–10981.
- (24) Zhou, Y.; Chen, J.; Bakr, O. M.; Sun, H.-T. Metal-Doped Lead Halide Perovskites: Synthesis, Properties, and Optoelectronic Applications. *Chem. Mater.* **2018**, *30* (19), 6589–6613.
- (25) Das Adhikari, S.; Guria, A. K.; Pradhan, N. Insights of Doping and the Photoluminescence Properties of Mn-Doped Perovskite Nanocrystals. *J. Phys. Chem. Lett.* **2019**, *10* (9), 2250–2257.
- (26) Milstein, T. J.; Kluherz, K. T.; Kroupa, D. M.; Erickson, C. S.; De Yoreo, J. J.; Gamelin, D. R. Anion Exchange and the Quantum-Cutting Energy Threshold in Ytterbium-Doped $CsPb(Cl_{1-x}Br_x)_3$ Perovskite Nanocrystals. *Nano Lett.* **2019**, *19* (3), 1931–1937.
- (27) Pan, G.; Bai, X.; Yang, D.; Chen, X.; Jing, P.; Qu, S.; Zhang, L.; Zhou, D.; Zhu, J.; Xu, W.; Dong, B.; Song, H. Doping Lanthanide into Perovskite Nanocrystals: Highly Improved and Expanded Optical Properties. *Nano Lett.* **2017**, *17* (12), 8005–8011.
- (28) van der Stam, W.; Geuchies, J. J.; Altantzis, T.; van den Bos, K. H. W.; Meeldijk, J. D.; Van Aert, S.; Bals, S.; Vanmaekelbergh, D.; de Mello Donega, C. Highly Emissive Divalent-Ion-Doped Colloidal

- $CsPb_{1-x}M_xBr_3$ Perovskite Nanocrystals through Cation Exchange. *J. Am. Chem. Soc.* **2017**, *139* (11), 4087–4097.
- (29) Parobek, D.; Roman, B. J.; Dong, Y.; Jin, H.; Lee, E.; Sheldon, M.; Son, D. H. Exciton-to-Dopant Energy Transfer in Mn-Doped Cesium Lead Halide Perovskite Nanocrystals. *Nano Lett.* **2016**, *16* (12), 7376–7380.
- (30) Liu, W.; Lin, Q.; Li, H.; Wu, K.; Robel, I.; Pietryga, J. M.; Klimov, V. I. Mn²⁺-Doped Lead Halide Perovskite Nanocrystals with Dual-Color Emission Controlled by Halide Content. *J. Am. Chem. Soc.* **2016**, 138 (45), 14954–14961.
- (31) Das Adhikari, S.; Dutta, S. K.; Dutta, A.; Guria, A. K.; Pradhan, N. Chemically Tailoring the Dopant Emission in Manganese-Doped CsPbCl₃ Perovskite Nanocrystals. *Angew. Chem., Int. Ed.* **2017**, *56* (30), 8746–8750.
- (32) Liu, H.; Wu, Z.; Shao, J.; Yao, D.; Gao, H.; Liu, Y.; Yu, W.; Zhang, H.; Yang, B. $CsPb_xMn_{1-x}Cl_3$ Perovskite Quantum Dots with High Mn Substitution Ratio. ACS Nano 2017, 11 (2), 2239–2247.
- (33) Huang, G.; Wang, C.; Xu, S.; Zong, S.; Lu, J.; Wang, Z.; Lu, C.; Cui, Y. Postsynthetic Doping of MnCl₂ Molecules into Preformed CsPbBr₃ Perovskite Nanocrystals via a Halide Exchange-Driven Cation Exchange. *Adv. Mater.* **2017**, *29* (29), 1700095.
- (34) Parobek, D.; Dong, Y.; Qiao, T.; Son, D. H. Direct Hot-Injection Synthesis of Mn-Doped CsPbBr₃ Nanocrystals. *Chem. Mater.* **2018**, 30 (9), 2939–2944.
- (35) Pinchetti, V.; Anand, A.; Akkerman, Q. A.; Sciacca, D.; Lorenzon, M.; Meinardi, F.; Fanciulli, M.; Manna, L.; Brovelli, S. Trap-Mediated Two-Step Sensitization of Manganese Dopants in Perovskite Nanocrystals. *ACS Energy Lett.* **2019**, *4* (1), 85–93.
- (36) Yuan, X.; Ji, S.; De Siena, M. C.; Fei, L.; Zhao, Z.; Wang, Y.; Li, H.; Zhao, J.; Gamelin, D. R. Photoluminescence Temperature Dependence, Dynamics, and Quantum Efficiencies in Mn²⁺-Doped CsPbCl₃ Perovskite Nanocrystals with Varied Dopant Concentration. *Chem. Mater.* **2017**, 29 (18), 8003–8011.
- (37) Dong, Y.; Qiao, T.; Kim, D.; Parobek, D.; Rossi, D.; Son, D. H. Precise Control of Quantum Confinement in Cesium Lead Halide Perovskite Quantum Dots via Thermodynamic Equilibrium. *Nano Lett.* **2018**, *18* (6), 3716–3722.
- (38) Rossi, D.; Liu, X.; Lee, Y.; Khurana, M.; Puthenpurayil, J.; Kim, K.; Akimov, A. V.; Cheon, J.; Son, D. H. Intense Dark Exciton Emission from Strongly Quantum-Confined CsPbBr₃ Nanocrystals. *Nano Lett.* **2020**, 20 (10), 7321–7326.
- (39) Rossi, D.; Qiao, T.; Liu, X.; Khurana, M.; Akimov, A. V.; Cheon, J.; Son, D. H. Size-dependent dark exciton properties in cesium lead halide perovskite quantum dots. *J. Chem. Phys.* **2020**, *153* (18), 184703.
- (40) Nirmal, M.; Norris, D. J.; Kuno, M.; Bawendi, M. G.; Efros, A. L.; Rosen, M. Observation of the "Dark Exciton" in CdSe Quantum Dots. *Phys. Rev. Lett.* **1995**, *75* (20), 3728–3731.
- (41) Tamarat, P.; Bodnarchuk, M. I.; Trebbia, J.-B.; Erni, R.; Kovalenko, M. V.; Even, J.; Lounis, B. The Ground Exciton State of Formamidinium Lead Bromide Perovskite Nanocrystals is a Singlet Dark State. *Nat. Mater.* **2019**, *18* (7), 717–724.
- (42) Xu, K.; Vliem, J. F.; Meijerink, A. Long-Lived Dark Exciton Emission in Mn-Doped CsPbCl₃ Perovskite Nanocrystals. *J. Phys. Chem. C* **2019**, *123* (1), 979–984.
- (43) Akkerman, Q. A.; Meggiolaro, D.; Dang, Z.; De Angelis, F.; Manna, L. Fluorescent Alloy $CsPb_xMn_{1-x}I_3$ Perovskite Nanocrystals with High Structural and Optical Stability. *ACS Energy Lett.* **2017**, 2 (9), 2183–2186.
- (44) De Siena, M. C.; Sommer, D. E.; Creutz, S. E.; Dunham, S. T.; Gamelin, D. R. Spinodal Decomposition During Anion Exchange in Colloidal $\mathrm{Mn^{2+}}$ -Doped $\mathrm{CsPbX_3}$ (X = Cl, Br) Perovskite Nanocrystals. *Chem. Mater.* **2019**, *31* (18), 7711–7722.
- (45) Becker, M. A.; Vaxenburg, R.; Nedelcu, G.; Sercel, P. C.; Shabaev, A.; Mehl, M. J.; Michopoulos, J. G.; Lambrakos, S. G.; Bernstein, N.; Lyons, J. L.; Stöferle, T.; Mahrt, R. F.; Kovalenko, M. V.; Norris, D. J.; Rainò, G.; Efros, A. L. Bright Triplet Excitons in Caesium Lead Halide Perovskites. *Nature* **2018**, *553* (7687), 189–193.

- (46) Sercel, P. C.; Lyons, J. L.; Wickramaratne, D.; Vaxenburg, R.; Bernstein, N.; Efros, A. L. Exciton Fine Structure in Perovskite Nanocrystals. *Nano Lett.* **2019**, *19* (6), 4068–4077.
- (47) Luo, B.; Naghadeh, S. B.; Zhang, J. Z. Lead Halide Perovskite Nanocrystals: Stability, Surface Passivation, and Structural Control. *ChemNanoMat* **2017**, *3* (7), 456–465.
- (48) Rainò, G.; Landuyt, A.; Krieg, F.; Bernasconi, C.; Ochsenbein, S. T.; Dirin, D. N.; Bodnarchuk, M. I.; Kovalenko, M. V. Underestimated Effect of a Polymer Matrix on the Light Emission of Single CsPbBr₃ Nanocrystals. *Nano Lett.* **2019**, *19* (6), 3648–3653.
- (49) Feldmann, S.; Gangishetty, M. K.; Bravić, I.; Neumann, T.; Peng, B.; Winkler, T.; Friend, R. H.; Monserrat, B.; Congreve, D. N.; Deschler, F. Charge Carrier Localization in Doped Perovskite Nanocrystals Enhances Radiative Recombination. *J. Am. Chem. Soc.* **2021**, *143* (23), 8647–8653.
- (50) Maes, J.; Balcaen, L.; Drijvers, E.; Zhao, Q.; De Roo, J.; Vantomme, A.; Vanhaecke, F.; Geiregat, P.; Hens, Z. Light Absorption Coefficient of CsPbBr₃ Perovskite Nanocrystals. *J. Phys. Chem. Lett.* **2018**, *9* (11), 3093–3097.
- (51) Puthenpurayil, J.; Cheng, O. H.-C.; Qiao, T.; Rossi, D.; Son, D. H. On the Determination of Absorption Cross Section of Colloidal Lead Halide Perovskite Quantum Dots. *J. Chem. Phys.* **2019**, *151* (15), 154706.
- (52) Chen, L.; Li, B.; Zhang, C.; Huang, X.; Wang, X.; Xiao, M. Composition-Dependent Energy Splitting between Bright and Dark Excitons in Lead Halide Perovskite Nanocrystals. *Nano Lett.* **2018**, *18* (3), 2074–2080.
- (53) Canneson, D.; Shornikova, E. V.; Yakovlev, D. R.; Rogge, T.; Mitioglu, A. A.; Ballottin, M. V.; Christianen, P. C. M.; Lhuillier, E.; Bayer, M.; Biadala, L. Negatively Charged and Dark Excitons in CsPbBr₃ Perovskite Nanocrystals Revealed by High Magnetic Fields. *Nano Lett.* **2017**, *17* (10), 6177–6183.
- (54) Neumann, T.; Feldmann, S.; Moser, P.; Delhomme, A.; Zerhoch, J.; van de Goor, T.; Wang, S.; Dyksik, M.; Winkler, T.; Finley, J. J.; Plochocka, P.; Brandt, M. S.; Faugeras, C.; Stier, A. V.; Deschler, F. Manganese Doping for Enhanced Magnetic Brightening and Circular Polarization Control of Dark Excitons in Paramagnetic Layered Hybrid Metal-halide Perovskites. *Nat. Commun.* **2021**, *12* (1), 3489.
- (55) Rossi, D.; Parobek, D.; Dong, Y.; Son, D. H. Dynamics of Exciton—Mn Energy Transfer in Mn-Doped CsPbCl₃ Perovskite Nanocrystals. *J. Phys. Chem. C* **2017**, *121* (32), 17143–17149.
- (56) Li, Z.-J.; Hofman, E.; Davis, A. H.; Khammang, A.; Wright, J. T.; Dzikovski, B.; Meulenberg, R. W.; Zheng, W. Complete Dopant Substitution by Spinodal Decomposition in Mn-Doped Two-Dimensional CsPbCl₃ Nanoplatelets. *Chem. Mater.* **2018**, *30* (18), 6400–6409.
- (57) Bhattacharyya, S.; Zitoun, D.; Gedanken, A. One-Pot Synthesis and Characterization of Mn²⁺-Doped Wurtzite CdSe Nanocrystals Encapsulated with Carbon. *J. Phys. Chem. C* **2008**, *112* (20), 7624–7630.